CHAPTER

7 Bacterial and fungal mediated synthesis, characterization and applications of AgNPs

S. Rajeshkumar[a], M. Jeevitha[b], D. Sheba[c], and M. Nagalingam[d]

[a]*Department of Pharmacology, Biomedical Research Unit and Laboratory Animal Research Centre, Saveetha Dental College and Hospitals, Saveetha Institute of Medical and Technical Sciences, Chennai, Tamil Nadu, India,*

[b]*Department of Periodontics, Saveetha Dental College, SIMATS, Saveetha University, Chennai, Tamil Nadu, India,*

[c]*PAPRSB Institute of Health Sciences, Universiti Brunei Darussalam, Gadong, Brunei Darussalam,*

[d]*Department of Bio-Chemistry, Indo-American College, Cheyyar, Tamil Nadu, India*

1 Introduction

Nanoparticles is an interesting field of research that has made a vital part of material science and biology recently owing to its excellent electrical, thermal, optical and biological properties. Silver is a precious metal with unique properties like high electrical and thermal conductivity and is applied in various fields such as medicine, electronics, jewelry, and catalytic process. The nanoparticles of silver which is in the size range of 1–100 nm has been shown to have antimicrobial, anticancer and wound healing properties (Siddiqi et al., 2018; Rajeshkumar and Naik, 2018; Santhoshkumar et al., 2017; Agarwal et al., 2017, 2018a,b; Grzelczak et al., 2008). The silver nanoparticles (AgNPs) are widely used as therapeutic agents, nanomedical imaging, food products, textiles and devices, water treatment, etc. (Firdhouse and Lalitha, 2015; Narayanan and Sakthivel, 2010; Vaidyanathan et al., 2009; Rai et al., 2012; Prabhu and Poulose, 2012; Rajeshkumar, 2016; Iravani et al., 2014; Siddiqi et al., 2018; Rajeshkumar and Bharath, 2017). Green synthesis of AgNPs is made possible from plants, bacteria, algae and fungi (Firdhouse and Lalitha, 2015; Rajeshkumar et al., 2012, 2013, 2014, 2016; Umayal et al., 2019). This review focusses on the plant, bacterial and fungal mediated synthesis, characterization and applications of AgNPs.

Agri-Waste and Microbes for Production of Sustainable Nanomaterials. https://doi.org/10.1016/B978-0-12-823575-1.00021-4

2 Green synthesis of AgNPs

Nanoparticles can be synthesized by various methods namely, physical methods, chemical methods and biological methods. AgNPs are synthesized by different chemical methods like solution reduction, electrochemical, photochemical reactions and pyrolysis (Agarwal et al., 2018a,b). The chemicals which are used commonly as reducing agents are ascorbic acid, alcohol, sodium citrate. These methods use toxic chemicals which are not eco-friendly. Physical methods involved are arc-discharge, energy ball milling method and direct current magnetron sputtering. These methods process faster than chemical methods but require much consumption of energy and need larger equipment which occupies more space (Siddiqi et al., 2018). Biological methods are more rapid and non-toxic.

2.1 Plant mediated synthesis

The plants are the most popularly used green approach for the AgNPs synthesis and the plant-mediated AgNPs are widely used in biomedical applications (Vanaja et al., 2013, 2014a,b; Menon et al., 2017; Paulkumar et al., 2014; Asha et al., 2017; Kanagavalli et al., 2016; Bhuyar et al., 2020; Umayal et al., 2019; Agarwal et al., 2018a,b; Rajeshkumar et al., 2013). Various plant mediated synthesis of AgNPs and its applications are listed (Table 1). Eco-friendly synthesis of AgNPs from an aqueous leaf extract of *Peganum harmala* was done by green approach. The reduction of silver ions was evident by the color change from pale yellow to brown. The synthesized AgNPs were characterized using UV-vis spectroscopy which showed semi-sharp peak at ~350 nm suggesting polydispersed nanoparticles formation (Alomar et al., 2020).

AgNPs were effectively biosynthesized utilizing *Cleome viscosa* plant extract, in a fast, eco-accommodating and a less expensive green synthesis method. *C. viscosa* fruit extract was used for synthesizing AgNPs, which diminishes silver nitrate into silver particles. The acquired AgNPs were characterized by UV, FT-IR, XRD, FE-SEM-EDAX and TEM examination. They were additionally examined for their natural exercises. The morphology of AgNPs was investigated utilizing SEM which depicted well dispersed spherical shape of the nanoparticles. The size of the nanoparticles was in the range of 20–50 nm, which was revealed by TEM. The green synthesized AgNPs displayed an effective antibacterial action against both Gram-negative and Gram-positive microbes. Besides, the green integrated AgNPs indicated substantial anticancer movement on the lung (A549) and ovarian (PA1) cancer cell lines with IC_{50} concentration at 28 and 30 µg/mL (Lakshmanan et al., 2018).

The AgNPs were biosynthesized from the leaf extract of *Hydnocarpus pentandra* and the antioxidant and cytotoxic effect of integrated AgNPs were tested against breast cancer cell line (MCF-7 cells). Characterization of AgNPs utilizing UV-vis spectrophotometry and SEM examination were performed. The UV-vis spectroscopy showed maximum absorption peak at 438 nm. The SEM images revealed the biosynthesized AgNPs to be spherical shaped with size range from 141 to 202 nm. The synthesized AgNPs were tested for antioxidant activity by DPPH method and cytotoxic

Table 1 Plant mediated synthesis, characterization and applications of AgNPs.

Plant name	Characterization (SEM, TEM, UV-vis, etc.)	Applications	References
Fruit extract of *Cleome viscosa*	• SEM revealed well defined spherical AgNPs • TEM indicated AgNPs size ranging from 20 to 50 nm • UV-vis spectroscopy indicated maximum absorption peak at 410–430 nm • FT-IR analysis showed maximum absorption at 539, 781, 1060, 1606, 2920 and 3420 cm^{-1} indicating the presence of plant biomolecules which act as capping agent for AgNPs • XRD spectra revealed the crystalline nature of AgNPs • EDAX analysis confirmed the presence of AgNPs	Antibacterial activity against *S. aureus* (17 ± 0.8 mm) followed by *E. coli* (16 ± 0.8 mm), *B. subtilis* (14 ± 1.5 mm) and *K. pneumoniae* (14 ± 1.2 mm) Anticancer activity against lung (A549) and ovarian (PA1) cancer cell lines	Lakshmanan et al. (2018)
Hydnocarpus pentandra leaf extract	• SEM showed spherical shape and size range from 141 to 202 nm • UV-vis spectroscopy indicated sharp peak at 438 nm	Antioxidant activity by DPPH method showed an effective antioxidant effect of AgNPs in a dose-dependent manner Cytotoxic activity against MCF-7 breast cancer cells also showed effective activity in a dose-dependent manner	Kumar et al. (2018a)
Moringa oleifera leaf extract	• SEM image revealed highly agglomerated AgNPs • TEM showed well dispersed, spherical shape with average sizes of 11 ± 4.3 and 9 ± 4.2 nm for freeze dried and fresh leaf mediated AgNPs • UV-vis spectroscopy showed maximum absorption peak at 450 and 440 nm, individually for both new and dried leaf samples • FT-IR spectra showed peaks at 3000–3300, 2800–3000, 1626, 1400–1550, 1380–1403 and 1000–1100 cm^{-1}	Antibacterial activity against *E. faecalis*, *P. aeruginosa* and *S. aureus* strains were sensitive to the synthesized AgNPs Antifungal activity against *Candida* which showed sensitivity at 6.25 $\mu g/mL^{-1}$	Moodley et al. (2018)
Leaf extract of *Punica granatum*	• SEM image revealed spherical, rhomboid, cubical shape and size range from 88 to 120 nm • UV-vis spectroscopy showed absorption peak at 255 and 450 nm • FT-IR spectra showed peak at 3633.69 cm^{-1}	—	Kumar et al. (2018b)
Origanum vulgare leaf extract	• TEM revealed the spherical shape and size range from 2 to 25 nm with average size of 12 nm • UV-vis spectroscopy revealed absorption peak at 430 nm • XRD analysis showed peak at 37.5° (111), 44.13° (200), 63.90° (220), 76.85° (311), and 81.13° (222) which indicated the crystalline nature of AgNPs • FT-IR spectra show peak at ~3389, ~2923, ~1595, and ~1072 cm^{-1} which indicated reducing and capping ability of *O. vulgare* leaf extract • EDX analysis confirmed the presence of AgNPs	Antibacterial activity against (*M. luteus*, *S. epidermidis*, Methicillin-resistant *Staphylococcus aureus* (MRSA), and *S. aureus*) Antifungal activity against pathogenic fungi (*A. flavus*, *A. alternate*, *P. variotii*) The zone of inhibition for bacterial strains was 12–19 nm and for fungal strains it was 12–28 nm	Shaik et al. (2018)

activity against breast cancer cell line MCF-7 and both of them showed potent activity in a dose-dependent manner (Kumar et al., 2018a,b).

The AgNPs synthesized using stem extract of *Phyllanthus pinnatus* were affirmed by surface plasmon resonance with an absorption peak at 490 nm. FT-IR revealed O–H stretch at 3316 cm^{-1}, C–H bond at 2918 cm^{-1} and 2850 cm^{-1} showing the involvement of hydroxyl groups in bioreduction process for synthesis of AgNPs. SEM image revealed AgNPs mostly in cubical shape and less in triangular and spherical shapes. XRD confirmed the crystalline nature of synthesized AgNPs (Balachandar et al., 2019).

AgNPs from the leaf extract of *Moringa oleifera* utilizing sunlight as an essential energy source, exhibited antimicrobial potential. Two different samples of AgNPs were synthesized, one sample from the fresh leaf material and the other sample obtained from freeze dried leaves. Silver nanoparticle synthesis was affirmed by surface plasmon resonance at 450 and 440 nm, individually for both fresh and dried leaf mediated AgNPs samples. SEM image revealed highly agglomerated AgNPs and the TEM image revealed well dispersed, spherical shape with average sizes of 11 ± 4.3 and 9 ± 4.2 nm for freeze dried and fresh leaf mediated AgNPs. FT-IR spectra showed peaks at 3000–3300, 2800–3000, 1626, 1400–1550, 1380–1403 and 1000–1100 cm^{-1} which indicated the presence of the functional groups. The biosynthesized AgNPs were tested for antibacterial activity against *E. faecalis*, *P. aeruginosa* and *S. aureus* strains and found to be sensitive to the nanoparticles and antifungal activity against *Candida* sp. showed sensitivity at 6.25 $\mu g/mL^{-1}$ concentration (Moodley et al., 2018).

AgNPs were synthesized using *Punica granatum* leaf extract and characterized using UV-vis spectroscopy, SEM and FT-IR analysis. The UV-vis spectroscopy revealed maximum absorption at 255 and 450 nm. The morphology of biosynthesized AgNPs was found to be spherical, rhomboid, cubical and size range from 88 to 120 nm. FT-IR spectra showed peak at 3633.69 cm^{-1} which indicate the capping and reducing ability of *Punica granatum* leaf extract (Kumar et al., 2018a,b).

AgNPs synthesized using *Origanum vulgare* leaf extract were characterized using UV-vis spectroscopy which showed a peak at 430 nm. XRD analysis indicated the crystalline nature of AgNPs. FT-IR spectra showed peak at ~3389, ~2923, ~1595 and ~1072 cm^{-1} which indicated the reducing and capping ability of *Origanum vulgare* leaf extract. The TEM image revealed the shape of AgNPs to be spherical in shape and size range from 2 to 25 nm with average size of 12 nm. The synthesized AgNPs were tested for antibacterial activity against disease causing bacteria (*M. luteus*, *S. epidermidis*, Methicillin-resistant *Staphylococcus aureus* (MRSA), and *S. aureus*) and antifungal activity against pathogenic fungi (*A. flavus*, *A. alternate* and *P. variotii*). The zone of inhibition for bacterial strains was found to be 12–19 nm and for fungal strains it was found to be 12–28 nm (Shaik et al., 2018).

2.2 Algae mediated synthesis

Different algae that are utilized in the synthesis of AgNPs and its applications are listed (Table 2). The AgNPs were synthesized by a green method using marine

Table 2 Algae mediated synthesis, characterization and applications of AgNPs.

Algae name	Characterization (SEM, TEM, UV-vis, etc.)	Applications	References
Macroalgae *Padina* spp.	• Size of AgNPs was found to be 33.75 nm from SEM image • UV-vis spectroscopy revealed maximum absorption peak at 445 nm • FT-IR analysis showed sharp peaks at 3350.07, 1637.74, and 1106.90 cm^{-1} and 3350.24, 1635.83, and 1337.47 cm^{-1} which indicate the presence of polyphenols and other functional groups present in the algae extract which acts as reducing and capping agent • FE-SEM showed aggregated AgNPs • EDAX analysis revealed peak at 2.8 and 8.0 keV which confirm the presence of AgNPs • The phytoconstituent was found to be cyclononasiloxane by GC-MS analysis	Antibacterial activity against *Staphylococcus aureus* and *Bacillus subtilis*, *Pseudomonas aeruginosa, Escherichia coli*, and *Salmonella typhi*. Among that *S. aureus* showed higher sensitivity to synthesized AgNPs (15.17 mm)	Bhuyar et al. (2020)
Sargassum longifolium	• SEM image revealed the shape of the nanoparticles to be spherical • TEM revealed mostly spherical and few in truncated and ellipsoidal in form • UV-vis spectroscopy showed a sharp peak at 460 nm • XRD value at 111 indicated the crystalline nature of AgNPs • FT-IR analysis confirmed the presence of functional groups that act as capping and reducing agent	Antifungal activity against *A. fumigatus*, *Fusarium* spp., *Candida albicans* *Fusarium* spp. showed higher antifungal activity up to 22.03 ± 0.033 mm	Rajeshkumar et al. (2014)
Caulerpa racemosa	• TEM revealed the size range from 5 to 25 nm • UV-vis spectroscopy showed maximum absorption peak at 413 nm • FT-IR spectra showed peaks at 3416, 2924, 2854, 1631, 1389, 1061, 1019 and 660 cm^{-1} which indicate the presence of functional groups • The XRD analysis confirmed the crystalline nature of synthesized AgNPs	Antibacterial activity against *Proteus mirabilis* which showed higher zone of inhibition (14 mm for 15 µL) than *S. aureus* (7 mm at 5 µL)	Kathiraven et al. (2015)
Pithophora oedogonia	• SEM image and DLS analysis revealed the size of AgNPs to be 34.03 nm • UV-vis spectroscopy showed an absorption peak at 445 nm • FT-IR spectra showed a peak at 3701, 3551, 2789, 2359 cm^{-1} indicates the capping and reducing the ability of the functional groups present in the algae extract • EDAX analysis confirmed the presence of AgNPs	Antibacterial activity against *Pseudomonas aeruginosa* (17.2 nm) and *Escherichia coli* (16.8 nm)	Sinha et al. (2015)
Sargassum cinereum	• SEM image revealed triangular nanoparticles with a size range from 45 to 60 nm • UV-vis spectroscopy showed absorption peak at 342–408 nm	Antibacterial activity against *S. aureus* with 2.5 µg/disc. The high antibacterial effect was shown by *Enterobacter aerogenes*, *Salmonella typhi*, *Proteus vulgaris* at 100 µg/disc	Mohandass et al. (2013)

microalgae *Padina* spp. The algae extract was used to synthesize AgNPs and characterized using UV-vis spectroscopy, which showed a maximum peak at 445 nm. The SEM image revealed that the size of AgNPs was about 33.75 nm. FT-IR analysis exhibited peaks at 3350.07, 1637.74, 1106.90, 3350.24, 1635.83 and 1337.47 cm^{-1} which indicated the presence of polyphenols and other functional groups present in the algae extract which acted as reducing and capping agent. FE-SEM showed aggregated AgNPs. EDAX analysis showed peaks at 2.8 and 8.0 keV which confirmed the presence of AgNPs. GC-MS analysis found the phytoconstituent to be cyclononasiloxane. Antibacterial activity against *Staphylococcus aureus*, *Bacillus subtilis*, *Pseudomonas aeruginosa*, *Escherichia coli*, and *Salmonella typhi* was tested. Among those *S. aureus* showed higher sensitivity to synthesized AgNPs (15.17 mm) (Bhuyar et al., 2020).

AgNPs synthesized using marine algae *Sargassum longifolium* as reducing agent were characterized using UV-vis spectroscopy, which showed a maximum peak at 460 nm. The SEM and TEM images revealed the shape of the nanoparticles to be spherical, truncated and ellipsoidal. XRD value at 111 indicated the crystalline nature of AgNPs. FT-IR analysis confirmed the presence of functional groups that acted as capping and reducing agent. Antifungal activity of synthesized AgNPs was tested against *A. fumigatus*, *Fusarium* spp., and *Candida albicans*. *Fusarium* spp. showed the highest antifungal activity up to 22.03 ± 0.033 mm (Rajeshkumar et al., 2014).

Caulerpa racemosa was the marine algae used to synthesize AgNPs. The UV-vis spectra showed maximum absorption peak at 413 nm. The TEM results depicted the size of AgNPs to be 5–25 nm. FT-IR spectra showed peaks at 3416, 2924, 2854, 1631, 1389, 1061, 1019 and 660 cm^{-1} which indicated the presence of functional groups. The XRD analysis confirmed the crystalline nature of synthesized AgNPs. Antibacterial activity against *Proteus mirabilis* showed higher zone of inhibition 14 mm for 15 µL than *S. aureus* that showed only 7 mm at 5 µL (Kathiraven et al., 2015).

Pithophora oedogonia (Mont.) Wittrock, a fresh water green algae, was used in an investigation to synthesize AgNPs and characterized using UV-vis spectroscopy which showed maximum absorption peak at 445 nm. SEM image and DLS analysis revealed the size of AgNPs to be 34.03 nm. FT-IR spectra showed peaks at 3701, 3551, 2789, 2359 cm^{-1} indicating the capping and reducing the ability of the functional groups present in the algae extract. EDAX analysis confirmed the presence of AgNPs. Positive antibacterial activity was found against *Pseudomonas aeruginosa* (17.2 mm) and *Escherichia coli* (16.8 mm) (Sinha et al., 2015). Biogenically synthesized AgNPs, using marine seaweed *Sargassum cinereum,* were tested for antibacterial activity. The UV-vis spectroscopy showed maximum absorption peak at 342–408 nm. The SEM results depicted the shape of the AgNPs to be triangular and size range from 45 to 60 nm. Antibacterial activity against *S. aureus* revealed 2.5 µg/disc. High antibacterial effect was shown by *Enterobacter aerogenes, Salmonella typhi, Proteus vulgaris* at 100 µg/disc (Mohandass et al., 2013).

2.3 Bacteria mediated synthesis of AgNPs

Biosynthesis of AgNPs utilizing microorganisms has got significant interest due to their capability to integrate nanoparticles of different size, shape and morphology. Different species of bacteria are used to biosynthesize AgNPs (Fig. 1). Various bacteria mediated AgNPs and its applications are enlisted (Table 3). AgNPs were synthesized by a bacterial strain (CS 11) confined from heavy metal polluted soil. Phylogenetic analysis of the 16S rDNA sequence of soil bacterial isolate *Bacillus* strain CS 11 demonstrated it as a strain of *Bacillus* species. The microscopic organisms with 1 mM $AgNO_3$, was found to be able to form AgNPs extracellularly at room temperature within 24 h. This was affirmed by the visual inspection and UV-vis absorption at 450 nm. Further characterization of biosynthesized AgNPs by TEM affirmed the size of AgNPs (Das et al., 2014).

The biosynthesis of AgNPs using endophytic microscopic organisms is a promising substitution for the chemical method. The investigation produced AgNPs utilizing endophytic bacterium *Bacillus siamensis* strain C1, which was secluded from the restorative plant *Coriandrum sativum*. The integrated AgNPs with the size of 25–50 nm were additionally affirmed and depicted by UV-vis spectroscopy, FT-IR, XRD, TEM and SEM with EDS analysis. The UV-vis spectroscopy showed maximum absorption peak at 400–450 nm. The TEM confirmed the spherical shape and SEM depicted the size of AgNPs that range from 25 to 50 nm. The XRD results showed the diffraction peaks at 2θ values of 27.81°, 32.34°, 46.29°, 57.47°, and 77.69° corresponding to (101), (111), (200), (220), and (311) crystal planes, respectively. The FT-IR spectra showed peaks at 1732 and 1645 cm^{-1} which indicated carbonyl extending

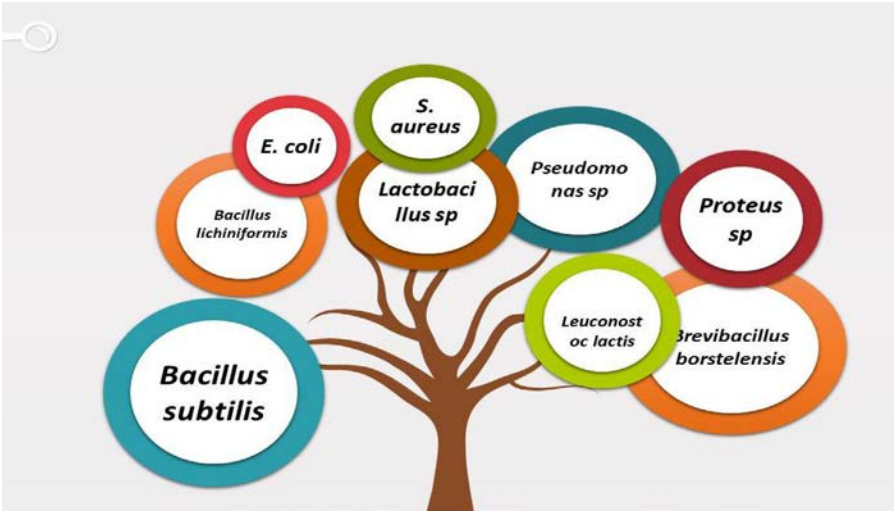

FIG. 1

Bacterial mediated zinc oxide nanoparticles.

Table 3 Bacteria mediated synthesis, characterization and applications of AgNPs.

Bacteria name	Characterization (SEM, TEM, UV-vis, etc.)	Applications	References
Bacillus strain CS 11 isolated from heavy metal contaminated soil	• TEM revealed spherical shape and size of about 42–94 nm • UV-vis spectroscopy showed maximum absorption at 450 nm	—	Das et al. (2014)
Bacillus siamensis strain C 1 (Ibrahim et al., 2019)	• SEM image indicated size of about 25–50 nm • TEM revealed spherical shaped particles • UV-vis spectroscopy showed peak at 400–450 nm • FT-IR showed peaks at 3385 and 2925 cm^{-1} indicating polysaccharides and C–H extending of alkanes, respectively. The peaks at 1732 and 1645 cm^{-1} indicating carbonyl extending vibration, while the peaks at 1556 and 1359 cm^{-1} indicative of (C–N) and (C–C) extending vibration of aromatic and aliphatic amines. The peaks at 1079 and 537 cm^{-1} indicating alkoxy group and the CH2 groups, respectively • EDS analysis showed the presence of 91.8% silver	Antibacterial activity—*Xanthomonas oryzae* pv. *oryzae* (Xoo) strain LND0005 and *Acidovorax oryzae (Ao) strain RS-1.* Moreover, the synthesized AgNPs altogether repressed bacterial development, biofilm arrangement and swimming motility of Xoo strain LND0005 and Ao strain RS-1	Ibrahim et al. (2019)
*Brevibacillus borstelensis*_ MTCC10642 (Kumar and Ghosh, 2016)	• SEM revealed monodispersed AgNPs and size range from 5 to 15 nm • UV-vis spectroscopy showed a sharp peak at 430 nm • FT-IR analysis indicated peak at 1345 cm^{-1} presence of nitrate in the residual solution • XRD showed prominent peaks at 320 (2θ), 460 (2θ), 570 (2θ), 760 (2θ) which indicate the crystalline nature of synthesized AgNPs		Kumar and Ghosh (2016)
Escherichia coli	• TEM revealed well disperse and size range from 20 to 50 nm • UV-vis spectroscopy indicated absorption peak at 400 nm	Antibacterial activity against *Bacillus subtilis* and *Klebsiella pneumonia* Growth curve assay	Kushwaha et al. (2015)
Lactobacillus strain LCM5	• TEM revealed polydisperse particles with an average size of 13.84 ± 4.56 nm • UV-absorption peak revealed at 420 nm	Antifungal activity against *Aspergillus flavus*, *Aspergillus ochraceus*, *Penicillium expansum* Antibacterial activity—*Chromobacterium violaceum*	Matei et al. (2020)
Leuconostoc lactis	• SEM image revealed spherical shape • TEM indicated spherical shape with average size of 35 nm • UV-vis spectroscopy showed maximum absorption peak at 425 nm • AFM, Raman spectroscopy and TGA analysis of AgNPs showed thermal stability at 437.1°C • XRD showed two diffraction peaks at 38.3° and 46.2° depicting the crystalline structure of metallic silver	In degradation of azo dyes like Methyl orange and Congo red	Saravanan et al. (2017)

Pseudoduganella eburnea MAHUQ-39	• FE-SEM revealed the bactericidal effect of the synthesized AgNPs against bacterial cells such as *Pseudomonas aeruginosa* and *Staphylococcus aureus* resulting in morphological changes and led to the lethality of the cell • TEM revealed size of AgNPs to be in the range of 8–24 nm • UV-vis spectroscopy showed maximum absorption peak at 448 nm • XRD and SAED confirmed the crystalline nature of AgNPs • EDX showed an absorption peak at 3 keV • FT-IR showed peaks at visible bands at 3439.16, 2922.29, 2854.13, 2360.07, 2342.06, 1734.23, 1636.01, 1457.49, and 1057.74 cm^{-1} which represent the biomolecules indulged in the synthesis of AgNPs	Antibacterial activity against *Staphylococcus aureus*, *Pseudomonas aeruginosa*. Minimum inhibitory concentration and Minimum Bactericidal concentration assay	Huq (2020)
Myxococcus virescens	• TEM revealed the size range of AgNPs to be 7–50 nm and showed polydisperse and spherical in shape • UV-vis spectroscopy indicated peak at 420 nm • Nanoparticle Track Analysis revealed the average size of about 81 nm and in suspension form to be 65 nm • FT-IR peak at 1051 cm^{-1} indicated the presence of AgNPs	Antibacterial activity against *Staphylococcus aureus* and *Pseudomonas aeruginosa*	Drzewiecka et al. (2014)
Thermophilic *Bacillus* sp. AZ1	• SEM image revealed size of AgNPs to be 7–31 nm • TEM indicated spherical shaped particles with a range from 9 to 32 nm • UV-vis spectroscopy showed maximum absorption peak at 425 nm • EXD analysis confirmed the presence of silver showing maximum absorption peak at 3 keV	Antimicrobial activity against two groups of the Gram-negative (*E. coli* and *S. typhi*) and Gram-positive organisms (*S. aureus* and *S. epidermidis*) *E. coli* is highly sensitive (22 nm) for biosynthesized AgNPs	Deljou and Goudarzi (2016)
Haemophilus influenzae	• Atomic Force Spectroscopy revealed spherical shaped biosynthesized AgNPs and size varied to the microbial medium used. Brain heart infusion broth (BHIB) and Tryptic soy broth (TSB) and incubation condition among synthesis of AgNPs—dark (D) and light (L) BHIBL—80.05 nm BHIBD—97.75 nm TSBL—95.54 nm TSBD—101.15 nm	Antibacterial activity against the Gram-negative *Escherichia coli*, *Pseudomonas aeruginosa*, *Klebsiella* sp., *Serratia* sp. and the Gram-positive bacteria *Staphylococcus aureus, Streptococcus* sp. and yeast *Candida albicans*	Ajah et al. (2018)
Pseudomonas aeruginosa KUPSB12	• SEM image revealed spherical shaped particles with a size range of 50–85 nm • UV-vis spectroscopy showed absorbance peak at 442 nm • FT-IR revealed peak at 1487.23 cm^{-1} indicating the presence of amine group	Antimicrobial activity against six pathogenic bacteria (*E. coli* MTCC 443, *Vibrio cholerae* MTCC 3904, *Shigella flexneri* MTCC 1457, *Bacillus subtilis* MTCC 441, *Staphylococcus aureus* MTCC 3160 and *Micrococcus luteus* MTCC 1538). *E. coli* showed higher zone of inhibition (19 mm)	Paul and Sinha (2014)

Continued

Table 3 Bacteria mediated synthesis, characterization and applications of AgNPs—cont'd

Bacteria name	Characterization (SEM, TEM, UV-vis, etc.)	Applications	References
Streptomyces sp. 09 PBT 005	• SEM image revealed particles in the size range of 198–595 nm • UV-vis spectroscopy showed the absorption peak at 440 nm • FT-IR showed peak at 1634 cm^{-1} confirmed the presence of the amide linkages of protein	Antibacterial activity against *S. flexneri* and *E. aerogenes*, *Klebsiella pneumoniae*, *S. typhimurium* and *S. typhi-B* and *P. vulgaris*, *Cytotoxic* activity using A549 lung cancer cell line showed 83.23% at 100 μL	Saravana Kumar et al. (2015)
Marine *Ochrobactrum* sp.	• TEM revealed spherical shaped particles in the size range of 35–85 nm • UV-vis spectroscopy showed an absorbance peak at 450 nm	Antibacterial activity against *Salmonella typhi*, *Salmonella paratyphi*, *Vibrio cholerae*, *Staphylococcus aureus*	Thomas et al. (2014)
Pseudomonas veronii AS41G	• UV-vis spectroscopy indicated maximum absorption peak at 410 nm • XRD confirmed the crystalline nature of AgNPs • FT-IR spectra showed an intense peak at 1400 cm^{-1} that correspond to stretching of carboxyl group. Stretching vibration at 1109 cm^{-1} indicated ketone and 1047 cm^{-1} indicated aliphatic amine	Antibacterial activity against *Bacillus subtilis* (MTCC 121), *Escherichia coli* (MTCC 7410), *Staphylococcus aureus* (MTCC 7443), *Klebsiella pneumonia* (MTCC 7407), *Pseudomonas aeruginosa* (MTCC 7903), *Xanthomonas axonopodis* pv. *Malvacearum*, *Xanthomonas oryzae* pv. *oryzae*, *Ralstonia solanacearum*	Baker et al. (2015)
Staphylococcus aureus	• UV-vis spectroscopy revealed absorption peak at 420 nm • AFM indicated particle size of 160–180 nm	Antibacterial activity against Methicillin resistant *Staphylococcus aureus,* which is more sensitive to biosynthesized AgNPs followed by Methicillin resistant *Staphylococcus epidermidis* and *Streptococcus pyogenes* Moderate antibacterial activity was observed in *Salmonella typhi* and *Klebsiella pneumonia*	Nanda and Saravanan (2009)

vibrations, while the peaks at 1556 and 1359 cm^{-1} depicted (C–N) and (C–C) extending vibrations of aromatic and aliphatic amines. The EDS analysis showed the presence of 91.8% silver (Ibrahim et al., 2019).

The synthesis of metal nanoparticles from microorganisms has currently become an extending research area because of their diverse and possible applications of the eco-friendly novel advancements. Synthesis of nanoparticles by chemical methods are very harmful, combustible in nature and their method of working is exploitative to the earth. Green approach of synthesizing AgNPs from silver nitrate utilized *Bacillus* sp.-*Brevibacillus borstelensis*_MTCC10642. The arrangement and characterization of AgNPs were affirmed by UV-vis spectroscopy, X-ray diffraction (XRD), Fourier Transform Infrared Spectroscopy (FT-IR), and Scanning Electron Microscopy (SEM). The SEM results revealed monodispersed AgNPs and size range from 5 to 15 nm. The UV-vis spectra showed its maximum absorption at 430 nm. FT-IR analysis peak at 1345 cm^{-1} indicated the presence of nitrate in the residual solution. XRD-showed prominent peaks at 320 (2θ), 460 (2θ), 570 (2θ), 760 (2θ) which indicated the crystalline nature of synthesized AgNPs (Kumar and Ghosh, 2016).

The utilization of microorganisms in the nanoparticle synthesis developed as an energizing methodology. Biosynthesis of AgNPs was done utilizing the bacterium *Escherichia coli*. The test bacterium confined from urine test was developed on EMB Agar medium and distinguished as *E. coli*. Biosynthesized nanoparticles were described by UV-vis spectroscopy and the most absorbance was found to be around 400 nm. The TEM results showed well dispersed AgNPs and their size range from 20 to 50 nm (Kushwaha et al., 2015).

Quick extracellular biosynthesis of AgNPs interceded by culture filtrate of lactic acid bacteria *Lactobacillus* sp. strain LCM5 was accomplished and transmission electron microscopy (TEM) results confirmed that the size of AgNPs by utilizing bacterial strain showed size in the range of 3–35 nm with normal particle size of 13.84 ± 4.56 nm (Matei et al., 2020).

AgNPs synthesized by using culture filtrate of *Leuconostoc lactis* bacteria were characterized using surface plasmon spectra utilizing UV-vis spectroscopy, XRD and Raman spectroscopy. The morphological characteristics of AgNPs were resolved through TEM, SEM and Atomic force microscopy (AFM), which demonstrated that the AgNPs were spherical shape, with an average size of 35 nm. The thermal conduct of AgNPs divulged that it was steady up to 437.1°C and the necessary energy was 808.2 J/g in TGA-DTA examination (Saravanan et al., 2017).

Resistance of pathogenic microorganisms to antimicrobial agents has developed as a major threat in recent days and also it is a significant medical issue. This report emphasized the synthesis of metallic nanoparticles of silver utilizing aqueous $Ag+$ particle with culture supernatants of *Staphylococcus aureus*. The biosynthesized AgNPs were characterized through UV-vis spectrophotometry and also by Atomic force microscopy. The UV-vis spectra showed maximum absorption peak at 420 nm. The atomic force microscopy analyzed the size of biosynthesized AgNPs to be from 160 to 180 nm (Nanda and Saravanan, 2009).

The green, fast, effortless, financially savvy and eco-friendly synthesis of AgNPs utilizing *Pseudoduganella eburnea* MAHUQ-39 was done and characterized by different methods. The UV-vis results showed maximum absorption peak at 448 nm. The transmission electron microscopy (TEM) picture uncovered spherical shape of the AgNPs. The size of the biosynthesized AgNPs was 8–24 nm. The Selected Area Electron diffraction (SAED) and X-ray diffraction (XRD) results uncovered the crystalline structure of AgNPs. Fourier-transform infrared spectroscopy (FT-IR) results demonstrated the presence of functional groups which were involved in the reduction of silver ions to AgNPs (Huq, 2020).

Extracellular synthesis of AgNPs of *Myxococcus virescens* was made possible by cell filtrate of the mycobacterium. The biosynthesized AgNPs from *M. virescens* cell filtrate were characterized by UV-vis spectroscopy, Nanoparticle Tracking Analysis (NTA) by LM 20, Zeta Potential investigation, Fourier Transform Infra-Red Spectroscopy (FT-IR) and Transmission Electron Microscopy (TEM). The UV-vis spectra showed the maximum absorption peak at 420 nm. The TEM results revealed the AgNPs size of about 7–50 nm, and exhibited polydisperse and spherical shape. Nanoparticle Track Analysis revealed the size of about 81 nm and in suspension form it is 65 nm. Zeta potential analysis was done to analyze the adsorption of OH ions on AgNPs and exhibited negative zeta potential. FT-IR-peak at 1051 cm^{-1} indicated the presence of AgNPs (Drzewiecka et al., 2014).

2.3.1 Applications of bacteria mediated synthesis of AgNPs

The biosynthesized AgNPs utilizing endophytic bacterium, *Bacillus siamensis* strain C1 demonstrated a resilient antibacterial impact at 20 µg/mL against the pathogen of rice bacterial leaf blight and bacterial brown stripe; while the zone of inhibition showed 17.3 and 16.0 mm for *Xanthomonas oryzae* pv. *oryzae* (Xoo) strain LND0005 and *Acidovorax oryzae* (Ao) strain RS^{-1}, respectively. Moreover, the synthesized AgNPs essentially restrained bacterial development, biofilm arrangement and swimming motility of Xoo strain LND0005 and Ao strain RS^{-1}. Also, the integrated AgNPs substantially expanded root length, shoot length, fresh weight and dry weight of rice seedlings contrasted with the control. These results showed that AgNPs can possibly secure rice plants from bacterial disease and induce growth of plant (Ibrahim et al., 2019).

The antibacterial effect of the biosynthesized AgNPs from the bacterium *Escherichia coli* was tested against microscopic organisms like *Bacillus subtilis* furthermore, *Klebsiella pneumonia*. Growth curve of organisms demonstrated considerable inhibition proving substantial antibacterial effect of the AgNPs (Kushwaha et al., 2015).

Antimicrobial action of AgNPs mediated by culture filtrate of lactic acid bacteria *Lactobacillus* sp. strain LCM5 was variable relying upon the two species and gathering of test microorganisms included. The zone of inhibition of *Aspergillus flavus* and *Aspergillus ochraceus* brought about by AgNPs integrated by lactic acid bacterial strain LCM5 were comparable (12.39 ± 0.61 and 12.86 ± 0.78 mm); however,

Penicillium expansum (15.87 ± 1.01 mm) was noted as sensitive. The effect of biosynthesized AgNPs was progressive against Gram-negative bacteria *Chromobacterium violaceum* with bigger zone of inhibition (18 ± 0.69 mm) when contrasted with those from fungi (Matei et al., 2020).

AgNPs biosynthesized using culture filtrate of *Leuconostoc lactis* bacteria evaluated for degradation capacity of azo dyes, for example, Methyl orange (MO) and Congo red (CR), demonstrated that AgNPs were seen as productive in encouraging the degradation procedure of industrial textile dyes. This makes biosynthesized AgNPs an appropriate, modest and condition agreeable contender for biodegradation of unsafe textile dyes (Saravanan et al., 2017).

The AgNPs biosynthesized from *Staphylococcus aureus* were assessed for their antimicrobial effect against distinctive pathogenic life forms. The antimicrobial action has been seen to be sensitive against methicillin-resistant *S. aureus* followed by methicillin-resistant *Staphylococcus epidermidis* and *Streptococcus pyogenes*, while just moderate antimicrobial effect was seen against *Salmonella typhi* and *Klebsiella pneumoniae* (Nanda and Saravanan, 2009).

The AgNPs biosynthesized from *Pseudoduganella eburnea* MAHUQ-39 showed substantial antimicrobial activity against multidrug-resistant pathogenic microbes. Minimum inhibitory concentration (MICs) of *Staphylococcus aureus* and *Pseudomonas aeruginosa* were 100 and 6.25 g/mL and the minimum bactericidal concentration (MBCs) of *S. aureus* and *P. aeruginosa* were 200 g/mL and 50 g/m, respectively. In this manner, AgNPs synthesized by strain MAHUQ-39 can be utilized as an efficient antimicrobial agent for different bio-remedial applications (Huq, 2020).

The antibacterial viability of AgNPs biosynthesized from cell filtrate of *Myxococcus virescens* was evaluated. The impact of AgNPs on survivability or lethality of human pathogenic microorganisms viz. *Staphylococcus aureus* (ATCC 6538), *Bacillus subtilis* subsp. *spizizenii* (ATCC 6633) and *Pseudomonas aeruginosa* (ATCC 10145) has been studied. Biosynthesized AgNPs exhibited promising cell lethality for these human pathogenic bacteria. This is a reasonable and basic procedure for synthesis of AgNPs which is having lethal properties against some clinical bacterial cell (Drzewiecka et al., 2014).

2.4 Fungal mediated synthesis of AgNPs

Numerous studies have been conducted on mycosynthesis of AgNPs using variety of species and strains of fungi. Fungal mediated synthesis is more favorable than that of bacteria is due to the large biomass formation in a short period in a laboratory at a faster rate and secretion of large amounts of proteins and enzymes. The exact mechanism of fungal mediated synthesis of AgNPs is not clear though the possible mechanism is suggested to be reduction of silver ions by the reduced form of nicotinamide adenine dinucleotide (NADH) and NADH-dependent nitrate reductase (Zomorodian et al., 2016). In recent times, using pesticides has shown to cause environmental and

FIG. 2

Different fungi used in silver nanoparticle synthesis.

health hazards. Endophytic fungi can produce natural bioactive compounds which can be an excellent alternative to plant based bioactive compounds that can be used for synthesis of AgNPs. Various fungi have been reported to synthesize AgNPs such as *Fusarium solani*, *Aspergillus fumigatus*, *Aspergillus clavatus*, *Aspergillus flavus*, *Aspergillus niger*, *Candida albicans* (Fig. 2). Many studies that reported fungal mediated biosynthesis of AgNPs and its applications are listed (Table 4).

3 Conclusion

Present book chapter clearly shows the biosynthesis of silver nanoparticles synthesized by using different bacterial strains. The characteristics of silver nanoparticles synthesized using various bacteria of different size, shape and crystalline nature. The fungal strains also synthesize the silver nanoparticles with different morphological characteristics. In that, the bacterial or fungal mediated nanoparticle synthesis is not having the same characters due to the presence of various primary and secondary metabolites present in the microbes which will be used in various biomedical applications. In future, the bacteria and fungal mediated silver nanoparticles may be used in different pharmaceutical, agricultural and multidisciplinary industries around the globe.

Table 4 Fungal mediated synthesis, characterization and applications of AgNPs.

Fungal name	Characterization (SEM, TEM, UV-vis, etc.)	Application	References
Fusarium solani	• SEM image revealed AgNPs size range from 5 to 30 nm • TEM revealed spherical and monodispersed particles • UV-vis spectroscopy indicated maximum absorption peak at 415 nm	Antifungal activity against corn, wheat and barley pathogens such as *F. moniliforme*, *F. verticillioides*, *A. flavus*, *A. niger*, *P. citrinum*, *P. chrysogenum*, *Phoma*, *A. chlamydospora*, *F. oxysporum*, *F. solani*, *F. semitectum*, *A. terreus*, *A. ficuum*, *P. islandicum*, *Rhizopus stolonifer*, *A. alternate*	El-aziz et al. (2015)
Aspergillus versicolor	• TEM revealed spherical shaped particles in the size range of 3–40 and 5–40 nm • UV-vis spectroscopy showed a peak at 429 nm • FT-IR showed peaks at 3273, 2925, 1629, 1320, 1020 cm^{-1} which indicated N–H stretching of the secondary amide, H stretching of methylene groups, CO stretch of amide I band, C–N stretching vibrations of aromatic amines, C–OH of the phenols. Particle size analyzer of AgNPs showed 15.5 nm, Zeta potential analyzer of AgNPs showed −38.2 mV	Free radical scavenging activity IC_{50} values is 60.64 μg/mL Antimicrobial activity against pathogens such as *Streptococcus pneumonia* (11.8 mm), *Staphylococcus aureus* (12.1 mm), *Klebsiella pneumonia* (13.6 mm), *Pseudomonas aeruginosa* (18.5 mm), *Candida nonalbicans* (13.6 mm) and *Candida albicans* (12.2 mm)	Netala et al. (2016)
Sclerotinia sclerotiorum	• TEM revealed spherical shaped particles with an average size of 10 nm • UV-vis spectroscopy showed a sharp peak at 430 nm • FT-IR showed peaks at 3223 and 3253 cm^{-1} which indicated N–H stretch of primary and secondary amines, 23,884 and 2390 cm^{-1} which indicate C≡N stretching vibrations 1762, 1719 and 1629 cm^{-1} which also confirmed the presence of primary amine	Antibacterial activity, minimum inhibitory concentration AgNPs against *E. coli* (20 mm) and *S. aureus* (19 mm)	Saxena et al. (2016)
Aspergillus fumigatus	• UV-vis spectroscopy showed an absorption peak at 430 nm • AFM revealed a spherical AgNPs size range of 5–95 nm		Zomorodian et al. (2016)
Aspergillus clavatus	• UV-vis spectroscopy showed an absorption peak at 430 nm • AFM indicated AgNPs of size range from 25 to 145 nm		Zomorodian et al. (2016)
Aspergillus niger	• UV-vis spectroscopy showed an absorption peak at 430 nm • AFM showed nanoparticles in the size range of 25–175 nm		Zomorodian et al. (2016)
Aspergillus flavus	• UV-vis spectroscopy showed an absorption peak at 430 nm • AFM revealed AgNPs size range of 45–185 nm		Zomorodian et al. (2016)
Aspergillus terreus	• TEM revealed AgNPs size range of 10–18 nm • UV-vis spectroscopy of AgNPs showed a peak at 430 nm • FT-IR indicated strong broad peak at 3462.56 cm^{-1}, dynamic light scattering be 11.85 nm for *A. terreus*, HPLC reduction were 58.87% and 52.18% for synthesized AgNPs	Antifungal activity showed inhibitory effect of AgNPs against mycelial growth of *A. ochraceus*, *A. niger* and *A. parasiticus*	Popli et al. (2018)

Continued

Table 4 Fungal mediated synthesis, characterization and applications of AgNPs—cont'd

Fungal name	Characterization (SEM, TEM, UV-vis, etc.)	Application	References
Penicillium expansum	• TEM indicated AgNPs size 14–25 nm • UV-vis spectroscopy showed an absorption peak at 430 nm • FT-IR resulted in strong, broad peak at 3449.06 cm^{-1}, dynamic light scattering found to be 25.73 • HPLC reductions were 58.87% and 52.18%, for synthesized AgNPs	Antifungal activity, inhibitory effect of AgNPs against mycelial growth of *A. ochraceus*, *A. niger* and *A. parasiticus*	Popli et al. (2018)
Trichoderma viride	• SEM observations showed AgNPs in the size range of 1–50 nm • TEM revealed spherical shaped AgNPs in size range from 1 to 50 nm • UV-vis spectroscopy detected extreme absorption peak at 620 nm • EDS spectrum confirmed that Ag was identified correctly	Antimicrobial activity against pathogenic bacteria such as MRSA (20 mm), *S. boydii* (28 mm), *A. baumannii* (23 mm), *S. sonnei* (21 mm) and *S. typhimurium* (25 mm)	Elgorban et al. (2016)
Curvularia tuberculata	• SEM revealed spherical shaped particles with a size range between 10 and 50 nm • UV-vis spectroscopy showed an absorbance peak at 420 nm	Antibacterial activity showed minimum inhibitory concentration and minimal bacterial concentration against pathogenic bacteria such as *E. coli*, *Proteus mirabilis*, *Pseudomonas aeruginosa*, *Salmonella typhi* and *Staphylococcus aureus*	Muhsin and Hachim (2015)
Candida albicans	• SEM image revealed spherical shaped particles with a size range of 50–100 nm • UV-vis spectroscopy revealed maximum absorbance peak at 400 nm • XRD analysis revealed the average grain size of the AgNPs to be 60 nm • Particle size analysis showed that maximum nanoparticles were in the range of 20–100 nm	Antimicrobial activity against multidrug resistant human pathogens like *E. coli*, *Klebsiella* sp., *Salmonella* sp., *Pseudomonas* sp. and *Staphylococcus aureus*	
Aspergillus fumigates	• SEM image revealed the size range of 15–38 nm • UV-vis spectroscopy revealed absorbance peak at 440 nm • The XRD analysis confirmed the average particle size of the silver to be 15–38 nm		Singh and Vidyasagar (2016)
Fusarium sp.	• SEM revealed the size range of 15–38 nm • UV-vis spectroscopy showed an absorbance peak at 440 nm • XRD analysis showed the average particle size of the silver to be 15–38 nm		Singh and Vidyasagar (2016)
Rhizopus spp.	• SEM revealed the size of the AgNPs in the range 15–38 nm • UV-vis spectroscopy absorbance peak at 440 nm • XRD analysis indicated the average particle size of the silver to be 15–38 nm		Singh and Vidyasagar (2016)

Aspergillus flavus	• SEM image revealed average size of 20 nm • TEM showed that most of the particles were spherical but some ellipsoidal and rod shaped • UV-vis spectroscopy revealed absorbance peak at 414 nm • FE-SEM revealed spherical, rod as well as irregular shaped and the size of particles is 48 nm • EDX showed absorption peak approximately at 2.5 keV		Behera et al. (2016)
Aspergillus niger	• SEM confirmed the average size of nanoparticles to be 60 nm • TEM indicated that most of the nanoparticles were spherical but some were ellipsoidal rod shaped • UV-vis spectroscopy showed the absorbance peak at 420 nm • FE-SEM detected spherical, rod as well as irregular shaped particles with an average size of 68 nm • EDX revealed absorption peak approximately at 2.5 keV		Behera et al. (2016)
Fusarium sp.	• TEM indicated spherical shaped particles in size ranging from 12 to 20 nm • UV-vis spectroscopy showed Surface Plasmon Resonance at 422 nm	Antibacterial activity of AgNPs against different pathogenic bacteria *E. coli*, *S. typhi* and *S. aureus*	Singh et al. (2015)
Verticillium	• SEM revealed particle size diameter of 12–25 nm • TEM showed spherical shaped nanoparticles • UV-vis spectroscopy revealed a broad absorption band centered at 450 nm • X-ray emission peak revealed at 3.1 keV		Mukherjee et al. (2001)
Candida glabrata	• TEM showed predominantly spherical and oval, well-dispersed uniform particles in the size range of 2–15 nm • UV-vis spectroscopy revealed single strong peak at 460.64 nm • FT-IR revealed a strong absorption line at 3436.03 cm^{-1}	Antibacterial activity against *S. aureus*, *E. coli*, *P. aeruginosa*, *K. pneumoniae*, *Salmonella typhimurium* and *Shigella flexneri* Antifungal activity against *Candia albicans*, *Candida tropicalis*, *Candida parapsilosis*, *Candida dubliniensis*, *Candida krusei* and *Candida glabrata*	Jalal et al. (2018)
Cladosporium species	• SEM revealed assembling, spherical and uniform AgNPs • UV-vis absorption peak observed at 438 nm • FT-IR showed strong peak absorption bands at 1042 cm^{-1} • X-ray diffraction analysis showed strong absorption in the range of 2.5–4 keV	Anti-cholinesterase activity anti-diabetic activity of α-amylase, α-glucosidase and dipeptidyl peptidase IV in vitro insulin sensitization and glucose uptake activity of AgNPs in different cell lines	Popli et al. (2018)
Botryosphaeria rhodina	• SEM showed uniform particle distribution • TEM revealed spherical shaped well dispersed particles with size ranging from 10 to 20 nm • UV-vis spectroscopy detected absorbance peak at 450 nm • FT-IR displayed absorption bands at 3303, 2967, 2156 cm^{-1} confirming the presence of capping and stabilizing agents	Toxic effect of AgNPs on cell viability after 48 h treatment; the increase in the concentration of nanoparticles decreases the viability of the cells in a dose-dependent manner Cytotoxic effect of AgNPs on A549 cells	Akther et al. (2019)

References

Agarwal, H., Venkat Kumar, S., Rajeshkumar, S., 2017. A review on green synthesis of zinc oxide nanoparticles—an eco-friendly approach. Resour. Technol. 3, 406–413.

Agarwal, H., Menon, S., Venkat Kumar, S., Rajeshkumar, S., 2018a. Mechanistic study on antibacterial action of zinc oxide nanoparticles synthesized using green route. Chem. Biol. Interact. 286, 60–70.

Agarwal, H., Venkat Kumar, S., Rajeshkumar, S., 2018b. Antidiabetic effect of silver nanoparticles synthesized using lemongrass (Cymbopogon citratus) through conventional heating and microwave irradiation approach. J. Microbiol. Biotechnol. Food Sci. 7, 371–376.

Ajah, H.A., Hassan, A.S., Aja, H.A., 2018. Extracellular biosynthesis of silver nanoparticles using *Fusarium graminearum* and their antimicrobial activity. J. Glob. Pharma Technol. 10, 683–689.

Akther, T., Mathipi, V., Kumar, N.S., Davoodbasha, M., 2019. Fungal-mediated synthesis of pharmaceutically active silver nanoparticles and anticancer property against A549 cells through apoptosis. Environ. Sci. Pollut. Res. 26, 13649–13657.

Alomar, T.S., AlMasoud, N., Awad, M.A., El-Tohamy, M.F., Soliman, D.A., 2020. An eco-friendly plant-mediated synthesis of silver nanoparticles: characterization, pharmaceutical and biomedical applications. Mater. Chem. Phys. 249, 123007.

Asha, S., Thirunavukkarasu, P., Rajeshkumar, S., 2017. Green synthesis of silver nanoparticles using Mirabilis jalapa aqueous extract and their antibacterial activity against respective microorganisms. Res. J. Pharm. Technol. 10, 811–817.

Baker, S., Mohan Kumar, K., Santosh, P., Rakshith, D., Satish, S., 2015. Extracellular synthesis of silver nanoparticles by novel Pseudomonas veronii AS41G inhabiting Annona squamosa L. and their bactericidal activity. Spectrochim. Acta A Mol. Biomol. Spectrosc. 136, 1434–1440.

Balachandar, R, Gurumoorthy, P, Karmegam, N, Barabadi, H, Subbaiya, R, Anand, K, Boomi, P, Saravanan, M, 2019. Plant-mediated synthesis, characterization and bactericidal potential of emerging silver nanoparticles using stem extract of *Phyllanthus pinnatus*: a recent advance in phytonanotechnology. J. Clust. Sci. 30 (6), 1481–1488.

Behera, A., Panda, S.S., Rout, N.C., Dhal, N.K., 2016. Biosynthesis of silver nanoparticles by fungi isolated from municipal waste contact. J. Afrikana 3 (2), 202–213.

Bhuyar, P., Rahim, M.H.A., Sundararaju, S., Ramaraj, R., Maniam, G.P., Govindan, N., 2020. Synthesis of silver nanoparticles using marine macroalgae Padina sp. and its antibacterial activity towards pathogenic bacteria. Beni Suef Univ. J. Basic Appl. Sci. 9, 1–5.

Das, V.L., Thomas, R., Varghese, R.T., Soniya, E.V., Mathew, J., Radhakrishnan, E.K., 2014. Extracellular synthesis of silver nanoparticles by the Bacillus strain CS 11 isolated from industrialized area. 3 Biotech 4, 121–126.

Deljou, A., Goudarzi, S., 2016. Green extracellular synthesis of the silver nanoparticles using thermophilic Bacillus sp. AZ1 and its antimicrobial activity against several human pathogenetic bacteria. Iran. J. Biotechnol. 14, 25–32.

Drzewiecka, W.W., Gaikwad, S., Laskowski, D., Dahm, H., Niedojadło, J., Gade, A., Rai, M., 2014. Novel approach towards synthesis of silver nanoparticles from Myxococcus virescens and their lethality on pathogenic bacterial cells. J. Biotechnol. Bioeng. 1, 1–7.

El-aziz, A., Mahmoud, M.A., Metwaly, H.A., 2015. Biosynthesis of silver nanoparticles using Fusarium solani. Dig. J. Nanomater. Biostruct. 10, 655–662.

Elgorban, A.M., Al-Rahmah, A.N., Sayed, S.R., Hirad, A., Mostafa, A.A., Bahkali, A.H., 2016. Antimicrobial activity and green synthesis of silver nanoparticles using Trichoderma viride. Biotechnol. Biotechnol. Equip. 30, 299–304.

Firdhouse, M.J., Lalitha, P., 2015. Biosynthesis of silver nanoparticles and its applications. J. Nanotechnol. 2015.

Grzelczak, M., Perez-Juste, J., Mulvaney, P., Liz-Marzan, L.M., 2008. Shape control in gold nanoparticle synthesis. Chem. Soc. Rev. 37, 1783–1791.

Huq, M.A., 2020. Green synthesis of silver nanoparticles using Pseudoduganella eburnea MAHUQ-39 and their antimicrobial mechanisms investigation against drug resistant human pathogens. Int. J. Mol. Sci. 21, 1510.

Ibrahim, E., Fouad, H., Zhang, M., Zhang, Y., Qiu, W., Yan, C., Li, B., Mo, J., Chen, J., 2019. Biosynthesis of silver nanoparticles using endophytic bacteria and their role in inhibition of rice pathogenic bacteria and plant growth promotion. RSC Adv. 9, 29293–29299.

Iravani, S., Korbekandi, H., Mirmohammadi, S.V., Zolfaghari, B., 2014. Synthesis of silver nanoparticles: chemical, physical and biological methods. Res. Pharm. Sci. 9, 385–406.

Jalal, M., Ansari, M.A., Alzohairy, M.A., Ali, S.G., Khan, H.M., Almatroudi, A., Raees, K., 2018. Biosynthesis of silver nanoparticles from oropharyngeal Candida glabrata isolates and their antimicrobial activity against clinical strains of bacteria and fungi. Nanomaterials 8, 586.

Kanagavalli, U., Sadiq, A.M., Rajeshkumar, S., 2016. Plant assisted synthesis of silver nanoparticles using Boerhaavia diffusa leaves extract and evolution of antibacterial activity. Res. J. Pharm. Technol. 9, 1064–1068.

Kathiraven, T., Sundaramanickam, A., Shanmugam, N., Balasubramanian, T., 2015. Green synthesis of silver nanoparticles using marine algae Caulerpa racemosa and their antibacterial activity against some human pathogens. Appl. Nanosci. 5, 499–504.

Kumar, A., Ghosh, A., 2016. Biosynthesis and characterization of silver nanoparticles with bacterial isolate from gangetic-alluvial soil. Int. J. Biotechnol. Biochem. 12, 95–102.

Kumar, K.K., Kumar, D.B., Punathil, R.R., 2018a. Green synthesis of silver nanoparticles using Hydnocarpus pentandra leaf extract: in-vitro cytotoxicity studies against MCF-7 cell line. J. Young Pharm. 10, 16–19.

Kumar, M., Dandapat, S., Ranjan, R., Kumar, A., Sinha, M.P., 2018b. Plant mediated synthesis of silver nanoparticles using Punica granatum aqueous leaf extract. J. Microbiol. Exp. 6, 175–178.

Kushwaha, A., Singh, V.K., Bhartariya, J., Singh, P., Yasmeen, K., 2015. Isolation and identification of E. coli bacteria for the synthesis of silver nanoparticles: characterization of the particles and study of antibacterial activity. J. Exp. Biol. 5, 65–70.

Lakshmanan, G., Sathiyaseelan, A., Kalaichelvan, P.T., Murugesan, K., 2018. Plant-mediated synthesis of silver nanoparticles using fruit extract of Cleome viscosa L.: assessment of their antibacterial and anticancer activity. Karbala Int. J. Mod. Sci. 4, 61–68.

Matei, A., Matei, S., Matei, G.M., Cogalniceanu, G., Cornea, C.P., 2020. Biosynthesis of silver nanoparticles mediated by culture filtrate of lactic acid bacteria, characterization and antifungal activity. Eurobiotech J. 4, 97–103.

Menon, S., Agarwal, H., Rajeshkumar, S., Venkat Kumar, S., 2017. Green synthesis of silver nanoparticles using medicinal plant Acalypha indica leaf extracts and its application as an antioxidant and antimicrobial agent against foodborne pathogens. Int. J. Appl. Pharm. 9, 42–50.

Mohandass, C., Vijayaraj, A.S., Rajasabapathy, R., Satheeshbabu, S., Rao, S.V., Shiva, C., De-Mello, I., 2013. Biosynthesis of silver nanoparticles from marine seaweed Sargassum cinereum and their antibacterial activity. Indian J. Pharm. Sci. 75, 606–610.

Moodley, J.S., Krishna, S.B.N., Pillay, K., Govender, P., 2018. Green synthesis of silver nanoparticles from Moringa oleifera leaf extracts and its antimicrobial potential. Adv. Nat. Sci. Nanosci. Nanotechnol. 9, 015011.

Muhsin, T.M., Hachim, A.K., 2015. Characterization and antibacterial efficacy of silver nanoparticles biosynthesized by the soil fungus Curvularia tuberculata. NanoSciTech Open Libr. 1, 1–5.

Mukherjee, P., Ahmad, A., Mandal, D., Senapati, S., Sainkar, S.R., Khan, M.I., Parishcha, R., Ajaykumar, P.V., Alam, M., Kumar, R., Sastry, M., 2001. Fungus-mediated synthesis of silver nanoparticles and their immobilization in the mycelial matrix: a novel biological approach to nanoparticle synthesis. Nano Lett. 1, 515–519.

Nanda, A., Saravanan, M., 2009. Biosynthesis of silver nanoparticles from Staphylococcus aureus and its antimicrobial activity against MRSA and MRSE. Nanomedicine 5, 452–456.

Narayanan, K.B., Sakthivel, N., 2010. Biological synthesis of metal nanoparticles by microbes. Adv. Colloid Interface Sci. 156, 1–13.

Netala, V.R., Kotakadi, V.S., Bobbu, P., Gaddam, S.A., Tartte, V., 2016. Endophytic fungal isolate mediated biosynthesis of silver nanoparticles and their free radical scavenging activity and antimicrobial studies. 3 Biotech 6, 1–9.

Paul, D., Sinha, S.N., 2014. Extracellular synthesis of silver nanoparticles using Pseudomonas aeruginosa KUPSB12 and its antibacterial activity. Jordan J. Biol. Sci. 7, 245–250.

Paulkumar, K., Gnanajobitha, G., Vanaja, M., Rajeshkumar, S., Malarkodi, C., Pandian, K., Annadurai, G., 2014. *Piper nigrum* leaf and stem assisted green synthesis of silver nanoparticles and evaluation of its antibacterial activity against agricultural plant pathogens. Sci. World J., 2014.

Popli, D., Anil, V., Subramanyam, A.B., Namratha, M.N., Ranjitha, V.R., Rao, S.N., Rai, R.V., Govindappa, M., 2018. Endophyte fungi, *Cladosporium* species-mediated synthesis of silver nanoparticles possessing in vitro antioxidant, anti-diabetic and anti-Alzheimer activity. Artif Cells Nanomed. Biotechnol. 46, 676–683.

Prabhu, S., Poulose, E.K., 2012. Silver nanoparticles: mechanism of antimicrobial action, synthesis, medical applications, and toxicity effects. Int. Nano. Lett. 2, 32.

Rai, M.K., Deshmukh, S.D., Ingle, A.P., Gade, A.K., 2012. Silver nanoparticles: the powerful nanoweapon against multidrug-resistant bacteria. J. Appl. Microbiol. 112, 841–852.

Rajeshkumar, S., 2016. Green synthesis of different sized antimicrobial silver nanoparticles using different parts of plants—a review. Int. J. ChemTech Res. 9, 197–208.

Rajeshkumar, S., Bharath, L.V., 2017. Mechanism of plant-mediated synthesis of silver nanoparticles—a review on biomolecules involved, characterisation and antibacterial activity. Chem. Biol. Interact. 273, 219–227.

Rajeshkumar, S., Malarkodi, C., Vanaja, M., Annadurai, G., 2016. Anticancer and enhanced antimicrobial activity of biosynthesized silver nanoparticles against clinical pathogens. J. Mol. Struct. 1116, 165–173.

Rajeshkumar, S., Naik, P., 2018. Synthesis and biomedical applications of cerium oxide nanoparticles—a review. Biotechnol. Rep. 17, 1–5.

Rajeshkumar, S., Jobitha, G.G., Malarkodi, C., Kannan, C., Annadurai, G., 2013. Optimization of marine bacteria Enterococcus sp. biomass growth by using response surface methodology. J. Environ. Nanotechnol. 2, 13–19.

Rajeshkumar, S., Kannan, C., Annadurai, G, 2012. Green synthesis of silver nanoparticles using marine brown *Turbinaria conoides* and its antibacterial activity. Int. J. Pharma Bio Sci. 3 (4), 502–510.

Rajeshkumar, S., Malarkodi, C., Paulkumar, K., Vanaja, M., Gnanajobitha, G., Annadurai, G., 2014. Algae mediated green fabrication of silver nanoparticles and examination of its antifungal activity against clinical pathogens. Int. J. Met. 2014, 1–8.

Santhoshkumar, J., Rajeshkumar, S., Venkat Kumar, S., 2017. Phyto-assisted synthesis, characterization and applications of gold nanoparticles—a review. Biochem. Biophys. Rep. 11, 46–57.

Saravana Kumar, P., Balachandran, C., Duraipandiyan, V., Ramasamy, D., Ignacimuthu, S., Al-Dhabi, N.A., 2015. Extracellular biosynthesis of silver nanoparticle using Streptomyces sp. 09 PBT 005 and its antibacterial and cytotoxic properties. Appl. Nanosci. 5, 169–180.

Saravanan, C., Rajesh, R., Kaviarasan, T., 2017. Synthesis of silver nanoparticles using bacterial exopolysaccharide and its application for degradation of azo-dyes. Biotechnol. Rep. 15, 33–40.

Saxena, J., Sharma, P.K., Sharma, M.M., Singh, A., 2016. Process optimization for green synthesis of silver nanoparticles by Sclerotinia sclerotiorum MTCC 8785 and evaluation of its antibacterial properties. Springerplus 5, 1–10.

Shaik, M.R., Khan, M., Kuniyil, M., Al-Warthan, A., Alkhathlan, H.Z., Siddiqui, M.R., Shaik, J.P., Ahamed, A., Mahmood, A., Khan, M., Adil, S.F., 2018. Plant-extract-assisted green synthesis of silver nanoparticles using Origanum vulgare L. extract and their microbicidal activities. Sustainability 10, 913.

Siddiqi, K.S., Husen, A., Rao, R.A.K., 2018. A review on biosynthesis of silver nanoparticles and their biocidal properties. J. Nanobiotechnol. 16, 1–28.

Singh, P.S., Vidyasagar, G.M., 2016. Biosynthesis of AgNPs with three widespread loam fungi via *Aspergillus fumigatus, Fusarium* spp*, Rhizopus* spp. J. Pharm. Med. Sci. 5, 33–36.

Singh, A.K., Rathod, V., Singh, D., Ninganagouda, S., Kulkarni, P., Mathew, J., Haq, M.U., 2015. Bioactive silver nanoparticles from endophytic fungus Fusarium sp. isolated from an ethanomedicinal plant *Withania somnifera* (Ashwagandha) and its antibacterial activity. Int. J. Nanomater. Biostruct. 5, 15–19.

Sinha, S.N., Paul, D., Halder, N., Sengupta, D., Patra, S.K., 2015. Green synthesis of silver nanoparticles using fresh water green alga *Pithophora oedogonia* (Mont.) Wittrock and evaluation of their antibacterial activity. Appl. Nanosci. 5, 703–709.

Thomas, R., Janardhanan, A., Varghese, R.T., Soniya, E.V., Mathew, J., Radhakrishnan, E.K., 2014. Antibacterial properties of silver nanoparticles synthesized by marine Ochrobactrum sp. Braz. J. Microbiol. 45, 1221–1227.

Umayal, S., Rajeshkumar, S., Vignesh, P., 2019. Comparative antibacterial analysis of fresh face cream, expired face cream, and papaya extract—an in vitro study. Drug Invent. Today 10, 13–17.

Vaidyanathan, R., Kalishwaralal, K., Gopalram, S., Gurunathan, S., 2009. Nanosilver—the burgeoning therapeutic molecule and its green synthesis. Biotechnol. Adv. 27, 924–937.

Vanaja, M., Gnanajobitha, G., Paulkumar, K., Rajeshkumar, S., Malarkodi, C., Annadurai, G., 2013. Phytosynthesis of silver nanoparticles by *Cissus quadrangularis*: influence of physicochemical factors. J. Nanostruct. Chem. 3, 1–8.

Vanaja, M., Paulkumar, K., Baburaja, M., Rajeshkumar, S., Gnanajobitha, G., Malarkodi, C., Sivakavinesan, M., Annadurai, G., 2014a. Degradation of methylene blue using biologically synthesized silver nanoparticles. Bioinorg. Chem. Appl. 2014, 1–8.

Vanaja, M., Paulkumar, K., Gnanajobitha, G., Rajeshkumar, S., Malarkodi, C., Annadurai, G., 2014b. Herbal plant synthesis of antibacterial silver nanoparticles by Solanum trilobatum and its characterization. Int. J. Met. 2014, 1–8.

Zomorodian, K., Pourshahid, S., Sadatsharifi, A., Mehryar, P., Pakshir, K., Rahimi, M.J., Monfared, A.A., 2016. Biosynthesis and characterization of silver nanoparticles by Aspergillus species. Biomed. Res. Int., 2016.